

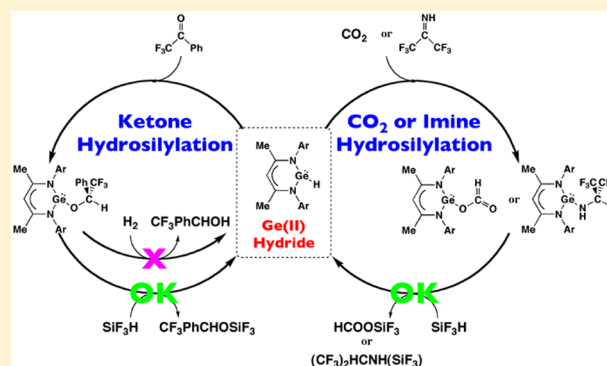
Theoretical Study of Reactivity of Ge(II)-hydride Compound: Comparison with Rh(I)-Hydride Complex and Prediction of Full Catalytic Cycle by Ge(II)-hydride

Nozomi Takagi and Shigeyoshi Sakaki*

Fukui Institute for Fundamental Chemistry, Kyoto University Takano, Nishihiraki-cho 34-4, Sakyo-ku, Kyoto 606-8103, Japan

S Supporting Information

ABSTRACT: The reaction of a Ge(II) hydride compound $\text{HC}\{\text{CMeArN}\}_2\text{GeH}$ ($\text{Ar} = 2,6\text{-iPr}_2\text{C}_6\text{H}_3$) **1** with 2,2,2-trifluoroacetophenone (CF_3PhCO) is theoretically investigated with density functional theory and spin-component-scaled second-order Møller–Plesset methods. This reaction easily occurs with moderate activation barrier and considerably large exothermicity, to afford a Ge(II) alkoxide **2** through a four-membered transition state. In the transition state, the charge transfer from the Ge–H σ -bonding molecular orbital (MO) to the $\text{C}=\text{O}$ π^* -antibonding MO of CF_3PhCO plays an important role. Acetone ($(\text{CH}_3)_2\text{CO}$) and benzophenone (Ph_2CO) are not reactive for **1**, because their π^* -antibonding MOs exist at higher energy than that of CF_3PhCO . Though **2** is easily formed, the catalytic hydrogenation of CF_3PhCO by **1** is difficult because the reaction of **2** with a dihydrogen molecule needs a large activation energy. On the other hand, our calculations clearly show that the catalytic hydrogenation of ketone by *cis*- $\text{RhH}(\text{PPh}_3)_2$ **4** easily occurs, as expected. The comparison of catalytic cycle between **1** and **4** suggests that the strong Ge–O bond of **2** is the reason of the very large activation energy for the hydrogenation by **1**. To overcome this defect, we investigated various reagents and found that the catalytic cycle can be completed with the use of SiF_3H . The product is silyl ether $\text{CF}_3\text{PhCHOSiF}_3$, which is equivalent to alcohol because it easily undergoes hydrolysis to afford CF_3PhCHOH . The similar catalytic cycles are also theoretically predicted for hydrosilylations of CO_2 and imine. This is the first theoretical prediction of the full catalytic cycle with a heavier main-group element compound.



INTRODUCTION

Activation of a small molecule is one of the important reactions of transition-metal complexes, because such activation is crucial as a key step of a catalytic reaction. Needless to say, the partially occupied valence d orbitals of a transition metal, which are usually close in energy, contribute to the activation. In this regard, it is believed that compounds of main-group element(s) cannot activate a small molecule, because the valence s and p orbitals of the main-group element construct bonding and antibonding molecular orbitals (MOs) at considerably separated energies.

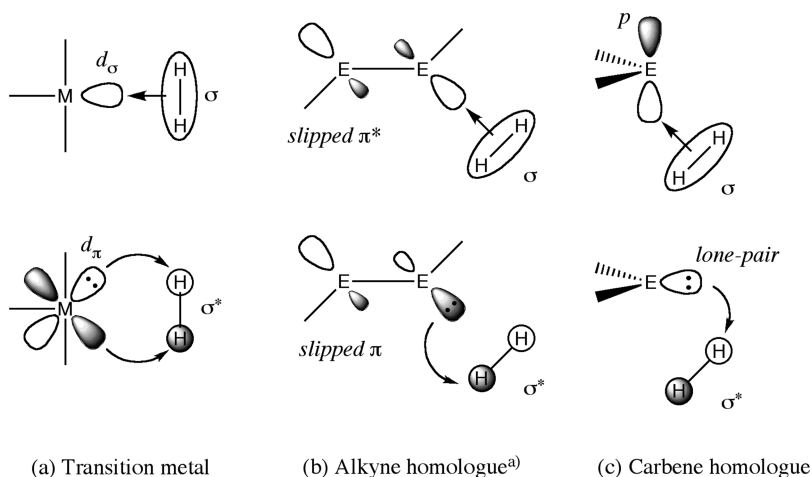
In the last 10 years, however, the situation has changed very much. Successful syntheses and isolations of novel compounds with heavier main-group elements, such as heavier homologues of ethylene,¹ acetylene,¹ benzene,² ketone,³ and carbene,⁴ have opened a new area of chemistry. In addition to their characteristic features in molecular structure and bonding interaction, some of these heavier compounds exhibit interesting reactivity for activation of such small molecules as dihydrogen,^{5–7} ammonia,^{6,8} carbon monoxide,⁹ carbon dioxide,^{8,10} and molecules containing $\text{C}=\text{C}$,¹¹ $\text{C}\equiv\text{C}$,⁸ $\text{N}=\text{N}$,¹² and $\text{C}-\text{H}$ ^{8,13} bonds. This means that the reactivities of these heavier compounds resemble those of transition-metal

complexes;¹⁴ see Scheme 1 for the schematic representation of dihydrogen activation by a transition-metal complex and a heavier main-group element compound. If a catalytic cycle is constructed with such heavier main-group element compounds, expensive transition-metal elements can be replaced with abundant main-group elements. At this moment, however, a catalytic cycle has not been successfully constructed yet with a heavier main-group element compound. For instance, a Ge(II) hydride compound $\text{HC}\{\text{CMeArN}\}_2\text{GeH}$ **1** ($\text{Ar} = 2,6\text{-iPr}_2\text{C}_6\text{H}_3$)¹⁵ reacts with CO_2 to afford a Ge(II) formate, as shown in Scheme 2a, which then reacts with a strong hydride source of LiH_2NBH_3 to reproduce **1** with the formation of lithium formate LiOCOH .^{16–18} However, this regeneration reaction was separately carried out from the first CO_2 activation under different conditions; in other words, the catalytic cycle has not been completed. Also, **1** reacts with ketone,^{16,19} alkyne,^{16,19,20} diazo-,^{16,19,21} and azo-compounds^{16,21} to produce the corresponding alkoxide, vinyl, and hydrazone compounds, respectively. However, no catalytic reaction has been reported in these cases too. On the other hand, transition-metal

Received: February 26, 2013

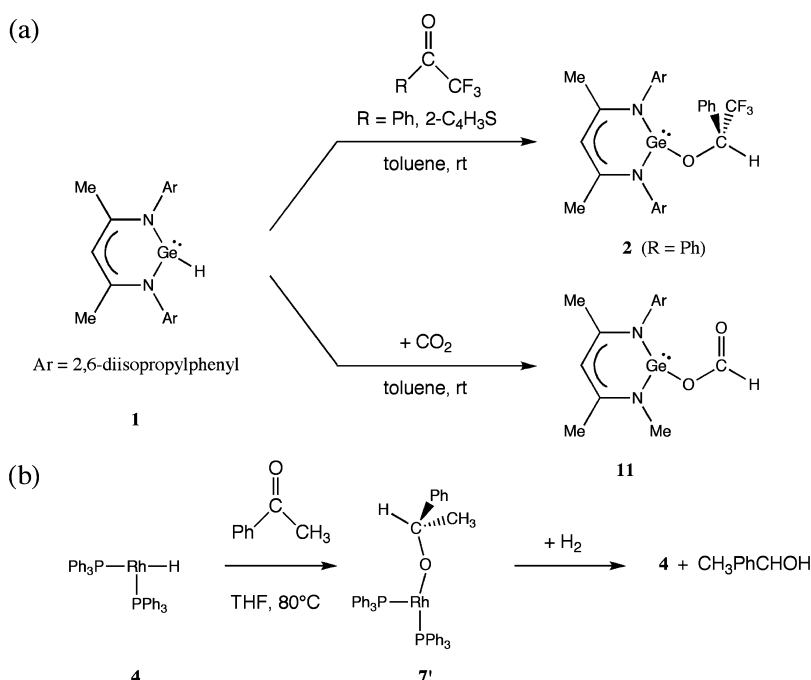
Published: May 23, 2013

Scheme 1. Schematic Representation of Dihydrogen Activation by (a) Transition-Metal Complex and (b) Alkyne and (c) Carbene Homologues



^aAnother π orbital perpendicular to the molecular plane is omitted for clarity.

Scheme 2. Experimentally Reported (a) Activation Reactions of Ketone and Carbon Dioxide by Ge(II) Hydride **1** and (b) Catalytic Hydrogenation Reaction of Ketone by Rh(I) Hydride **4**



complexes are effective for catalytic conversion reactions of these small molecules, as well-known. For instance, the catalytic hydrogenation, racemization, and hydrogen-transfer reactions of ketone and alcohol are successfully performed with a Rh(I) hydride complex (Scheme 2b).^{22,23} One can expect that comparisons of reactivity, reaction mechanism, electronic process, and catalytic activity between the Ge(II) and Rh(I) hydrides provide a good idea how to construct a catalytic cycle with a compound of heavier main-group element.

The reactivities of several heavier main-group element compounds have been theoretically investigated to elucidate the reaction mechanism and electronic process.^{6,11b,13c,24–26} For instance, the density functional theory (DFT) study of H–H σ -bond activation of a dihydrogen molecule and N–H σ -bond activation of ammonia by unsaturated Ge and Sn

compounds reported that the interaction between the H–H σ -bonding MO and the 4p(Ge) or 5p(Sn) orbital plays important role in the reaction as well as the back-donation from the Ge or Sn lone-pair MO to the H–H σ^* -antibonding MO.⁶ The similar N–H σ -bond activation of hydrazine with an unsaturated Ge compound was investigated with the DFT method.²⁴ The H–H σ -bond activation of a dihydrogen molecule by acetylene homologues of Ge and Sn²⁵ and dimetallenes (E = Al or Ga)²⁶ were theoretically investigated with the ONIOM(CCSD(T):DFT) and DFT methods, respectively. These studies disclosed that the inert-element multiple bond plays a crucial role in the reaction. The reaction mechanism of the reduction of CO₂ to CO with an amido-digermene was also investigated by the DFT method.¹⁰ However, no theoretical work has discussed similarities and/

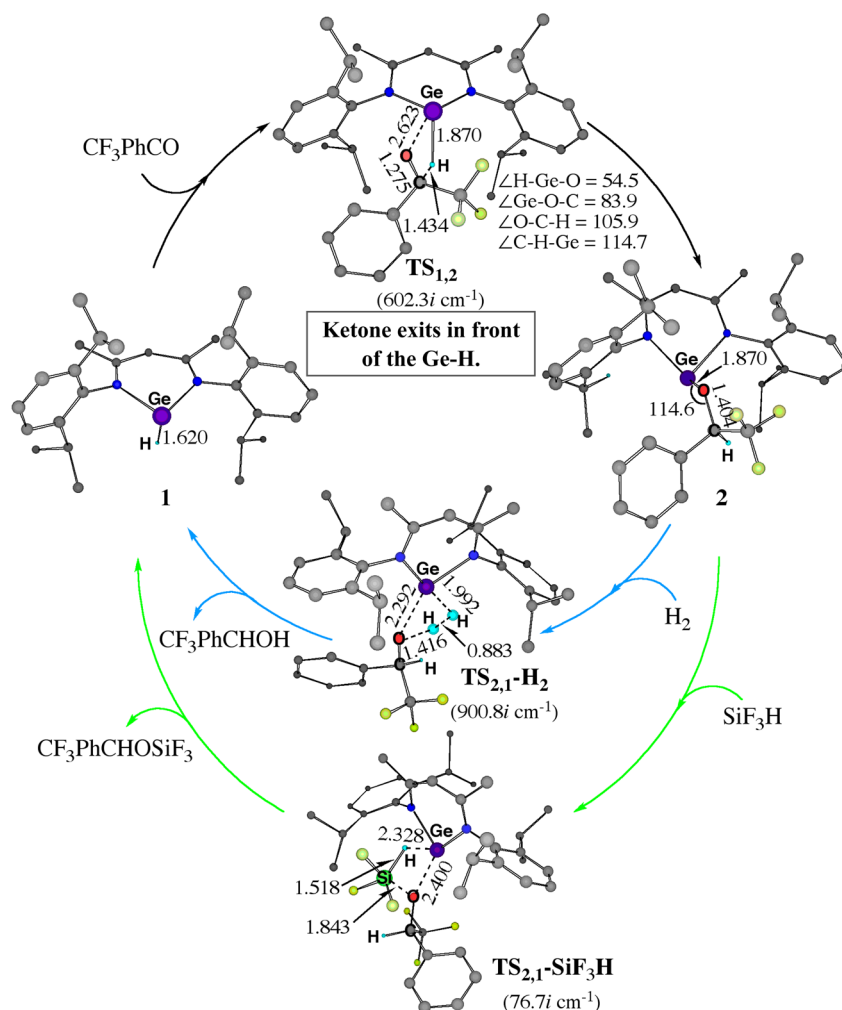


Figure 1. Geometry changes in hydrogenation and hydrosilylation of CF₃PhCO by the Ge(II) hydride **1**. B3PW91/BS-1 level. Hydrogen atoms are omitted for clarity. Distances and angles are in Å and degrees, respectively.

or differences in reactivity between a heavier main-group element compound and a transition-metal complex yet.

In this work, we theoretically investigated the reaction of **1** with ketone to afford a corresponding Ge(II) alkoxide **2** (Scheme 2a), which was reported by the recent experiments.^{16,19} Though this reaction is the same as the initial step of the hydrogenation of ketone by a Rh(I) hydride complex *cis*-RhH(PPh₃)₂ **4** (Scheme 2b),^{22,23} catalytic hydrogenation of ketone with **1** has not succeeded. Our purposes here are to clarify the mechanism and the electronic process of the reaction of **1** with ketone, to show similarities and/or differences in reactivity between **1** and **4**, and to provide a theoretical prediction how to construct catalytic cycles for transformations of ketone, carbon dioxide, and imine by **1**. We wish to emphasize that this is the first theoretical prediction of the full catalytic cycle with a compound of heavier main-group element.

■ COMPUTATIONAL DETAILS

The real Ge(II) hydride compound **1** bearing two bulky aryl groups (Ar = 2,6-diisopropylphenyl) and Rh(I) hydride *cis*-RhH(PPh₃)₂ **4** were employed in the calculations. Though a dimeric species of a Ge(II) hydride compound was reported previously,²⁷ the dimerization of **1** is difficult because the bulky

chelate ligand HC{CMeArN}₂ coordinates with the Ge center; see Figure S9g.

All geometries were optimized by the DFT method with the B3PW91 functional.^{28,29} For Ge, the LANL2DZ basis set was employed with one d polarization function,³⁰ where the core electrons were replaced with the effective core potentials (ECPs).³⁰ For Rh, the LANL2DZ basis set was employed with the ECPs.³⁰ The 6-31G(d) basis sets were employed for other atoms,³¹ where one diffuse function was added to O and one p polarization function was added to H atoms of hydride, dihydrogen, and silane. This basis set system is denoted as BS-1. At this level, the experimentally reported X-ray structures of the Ge(II) hydride **1** and the Ge(II) alkoxide **2** were well reproduced; see Table S1. A better basis set system, denoted as BS-2, was employed for the analysis of the electron population and the evaluation of energy changes. In BS-2, the SDB-cc-pVTZ basis sets³² were employed for Ge with the ECPs of the Stuttgart–Dresden–Bonn group.³³ A (311111/22111/411/11) basis set was employed for Rh with the SDB ECPs.^{33,34} The 6-311G(d) basis sets were employed for other elements, where one diffuse function was added to O and one p polarization function was added to H atoms of hydride, dihydrogen, and silane.

The energy changes were evaluated with the spin-component-scaled MP2 (SCS-MP2) method.³⁵ The reliability

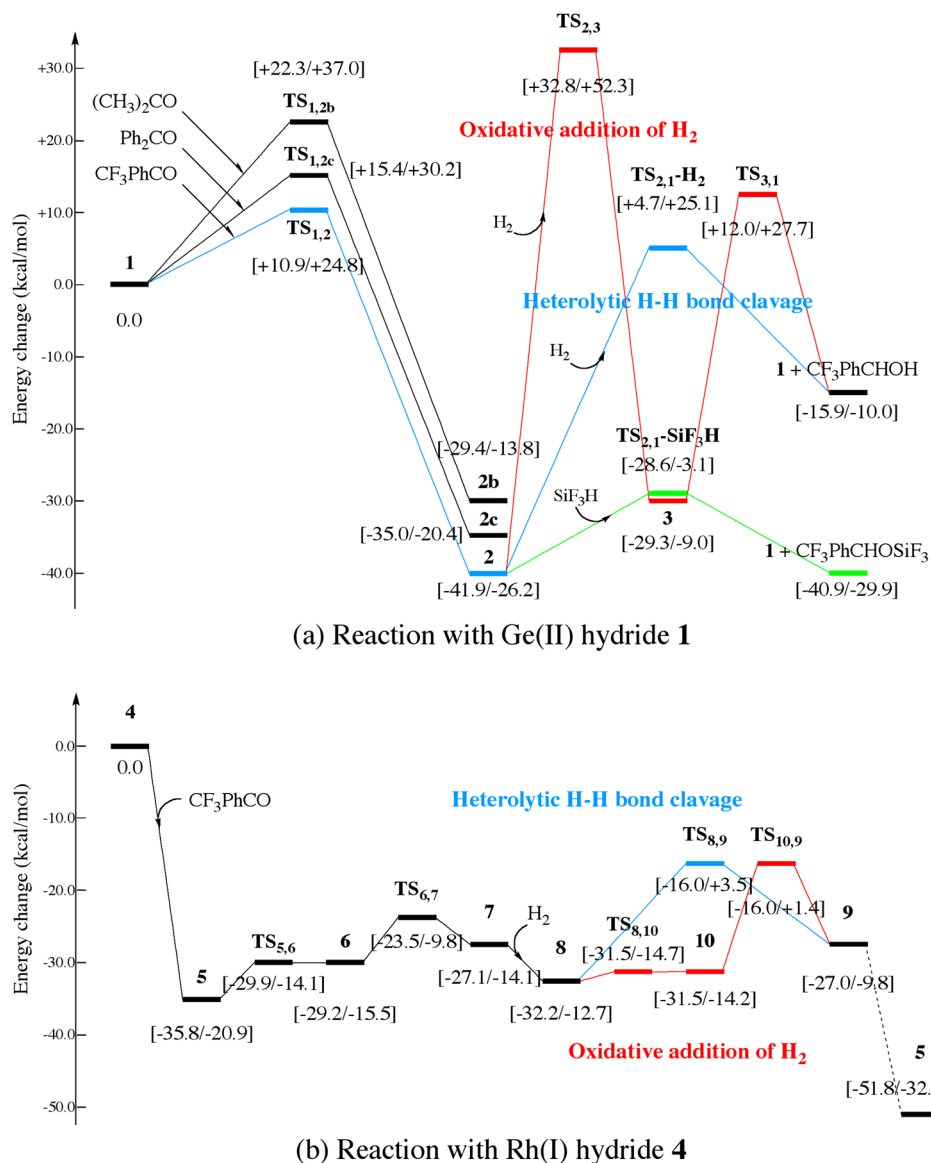


Figure 2. Potential (ΔE) and Gibbs (ΔG^0) energy changes (in kcal/mol) in (a) the hydrogenation and hydrosilylation of CF_3PhCO by the Ge(II) hydride 1 and (b) the hydrogenation of CF_3PhCO by the Rh(I) hydride 4 at the SCS-MP2/BS-2//B3PW91/BS-1 level, where ΔE and ΔG^0 are shown before and after the slash, respectively. For the Gibbs energy, solvation effect (in toluene for (a) and THF for (b)) is considered with the PCM method. The translational entropy was corrected with the method developed by Whitesides et al.³⁷

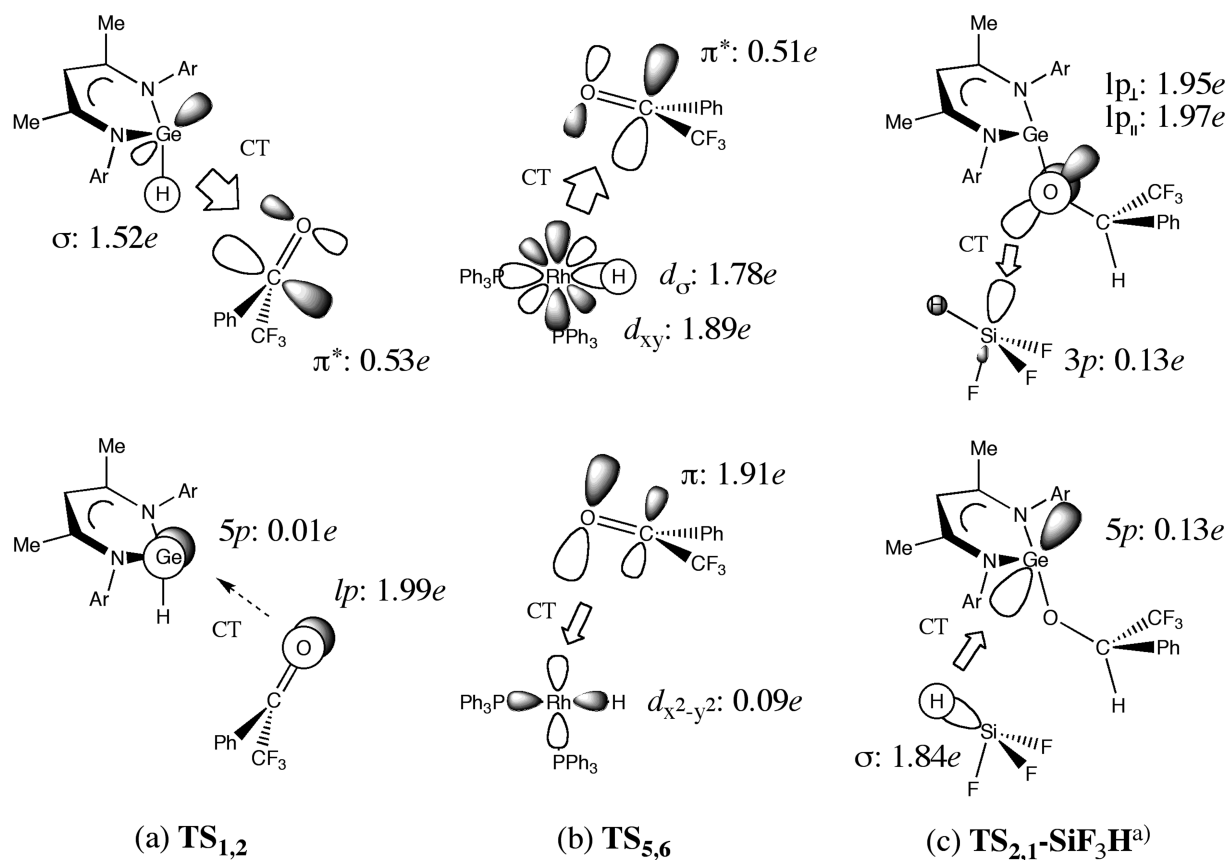
of this method was checked by comparing the SCS-MP2 calculated energy changes with the MP4(SDQ) and CCSD(T)-calculated values in a model system; see Tables S2 and S3. The potential energy including the zero-point energy correction is presented here. The Gibbs energy in solvent was calculated with the polarized continuum model (PCM),³⁶ where the translational entropy was corrected with the method developed by Whitesides et al.;³⁷ see page S2 in the Supporting Information for the details. The electron population analysis was carried out with the electron density at the MP2 level. All calculations were carried out with the Gaussian09 program package.³⁸

RESULTS AND DISCUSSION

Activation of Ketone with Ge(II) Hydride Compound

1. Recent experiments show that 1 reacts with 2,2,2-trifluoroacetophenone (CF_3PhCO) in toluene at room temperature to quantitatively produce a corresponding Ge(II) alkoxide

2.^{16,19} The present theoretical calculations show that this reaction occurs in the less congested front side of 1 via a four-membered transition state $\text{TS}_{1,2}$ to afford 2, as shown in Figure 1. The shorter C...H distance (1.434 Å) and the longer Ge...O distance (2.623 Å) in $\text{TS}_{1,2}$ suggest that the ketone activation is mainly initiated by the interaction between the hydride of 1 and the carbonyl carbon of CF_3PhCO . As shown in Figure 2a, the activation energy (E_a) and the Gibbs energy of activation ($\Delta G^{0\ddagger}$) are calculated to be 10.9 and 24.8 kcal/mol, respectively, and the reaction energy (ΔE) and the Gibbs energy of reaction (ΔG^0) are -41.9 and -26.2 kcal/mol. This large exothermicity arises from the formation of the strong Ge-O bond in 2, which will be discussed below. Here, we wish to mention the difference between 1 and ArGeH (Ar = aromatic ligand). The energetics of the intermediate 2 would be less favorable than that of ArGeH ,²⁷ because the bidentate $\text{HC}\{\text{CMeArN}\}_2$ ligand coordinates with the Ge center through electron-withdrawing N atoms.



charge-transfer interaction

Figure 3. Schematic view of CT interaction and electron population in interacting fragments in (a) $TS_{1,2}$, (b) $TS_{5,6}$, and (c) $TS_{2,1}-SiF_3H^a$.

The highest occupied molecular orbital (HOMO) of $TS_{1,2}$ mainly consists of the Ge–H σ -bonding MO (HOMO) of **1** and the C=O π^* -antibonding MO (LUMO) of CF_3PhCO ; see Figure 3a. The electron population of the HOMO of the Ge moiety decreases from $2.0e$ to $1.52e$ and that of the LUMO of the CF_3PhCO moiety increases to $0.53e$ in $TS_{1,2}$; see page S3 in the Supporting Information for the details of the population analysis. These results show that the charge transfer (CT) significantly occurs from **1** to CF_3PhCO in $TS_{1,2}$. On the other hand, the CT from CF_3PhCO to **1** occurs little, as shown by the very small electron population of the $5p$ orbital (LUMO+6) of the Ge center ($0.01e$) and the very small population change on the oxygen lone-pair MO (HOMO-2) of the CF_3PhCO moiety ($1.99e$). This is because the valence orbitals of the Ge atom are fully occupied. Interestingly, the lone-pair MO (HOMO-1) of **1** contributes little to this activation reaction. These results are consistent with the structural features of $TS_{1,2}$ that the C \cdots H distance is short (1.434 \AA) and the Ge \cdots O distance is long (2.623 \AA).

The reactions of **1** with $(CH_3)_2CO$ and Ph_2CO are also investigated, where the corresponding alkoxides **2b** and **2c** are produced, respectively. It was experimentally reported that CF_3PhCO is reactive to **1**, but $(CH_3)_2CO$ and Ph_2CO are not.^{16,19} The geometries of the transition states ($TS_{1,2b}$ and $TS_{1,2c}$) of these reactions are considerably different from that of $TS_{1,2}$, as shown in Figure S1. For instance, the C \cdots H distance in the transition state becomes longer in the order of CF_3PhCO (1.434 \AA) < Ph_2CO (1.457 \AA) < $(CH_3)_2CO$ (1.481 \AA), and the

Ge \cdots O distance becomes shorter in the order of CF_3PhCO (2.623 \AA) > Ph_2CO (2.352 \AA) > $(CH_3)_2CO$ (2.269 \AA). The same order is observed for the activation energy; the E_a and $\Delta G^{0\ddagger}$ values are 22.3 and 37.0 kcal/mol for $(CH_3)_2CO$, which are much larger than those for CF_3PhCO , as shown in Figure 2a. The E_a and $\Delta G^{0\ddagger}$ values (15.4 and 30.2 kcal/mol) for Ph_2CO are also larger than those for CF_3PhCO . These results are consistent with the experimental results that **1** is reactive to CF_3PhCO but not to $(CH_3)_2CO$ and Ph_2CO . The ΔE and ΔG^0 of $(CH_3)_2CO$ and Ph_2CO are less exothermic than that of CF_3PhCO . These geometrical features and reactivities arise from the C=O π^* -antibonding MO energy of ketone, as will be discussed below.

The CT from the Ge–H σ -bonding MO of **1** to the C=O π^* -antibonding MO of ketone plays a crucial role in this reaction. The electron population of the Ge–H σ -bonding MO is $1.72e$ for $(CH_3)_2CO$ and $1.64e$ for Ph_2CO . These results indicate that the CT becomes smaller in the order of CF_3PhCO > Ph_2CO > $(CH_3)_2CO$. The electron populations of the C=O π^* -antibonding MOs of $(CH_3)_2CO$ ($0.47e$) and Ph_2CO ($0.43e$) are considerably smaller than that of CF_3PhCO ($0.53e$). The reason is easily interpreted in terms of the C=O π^* -antibonding MO energy of ketone; it becomes higher in the order of CF_3PhCO ($+1.25 \text{ eV}$) < Ph_2CO ($+1.76 \text{ eV}$) < $(CH_3)_2CO$ ($+3.84 \text{ eV}$). As a result, the ΔE_a and $\Delta G^{0\ddagger}$ increase, and the C \cdots H distance becomes longer in the same order. Though the CT from the lone-pair MO of $(CH_3)_2CO$ ($0.03e$) and Ph_2CO ($0.02e$) to the vacant $5p$ orbital of the Ge is

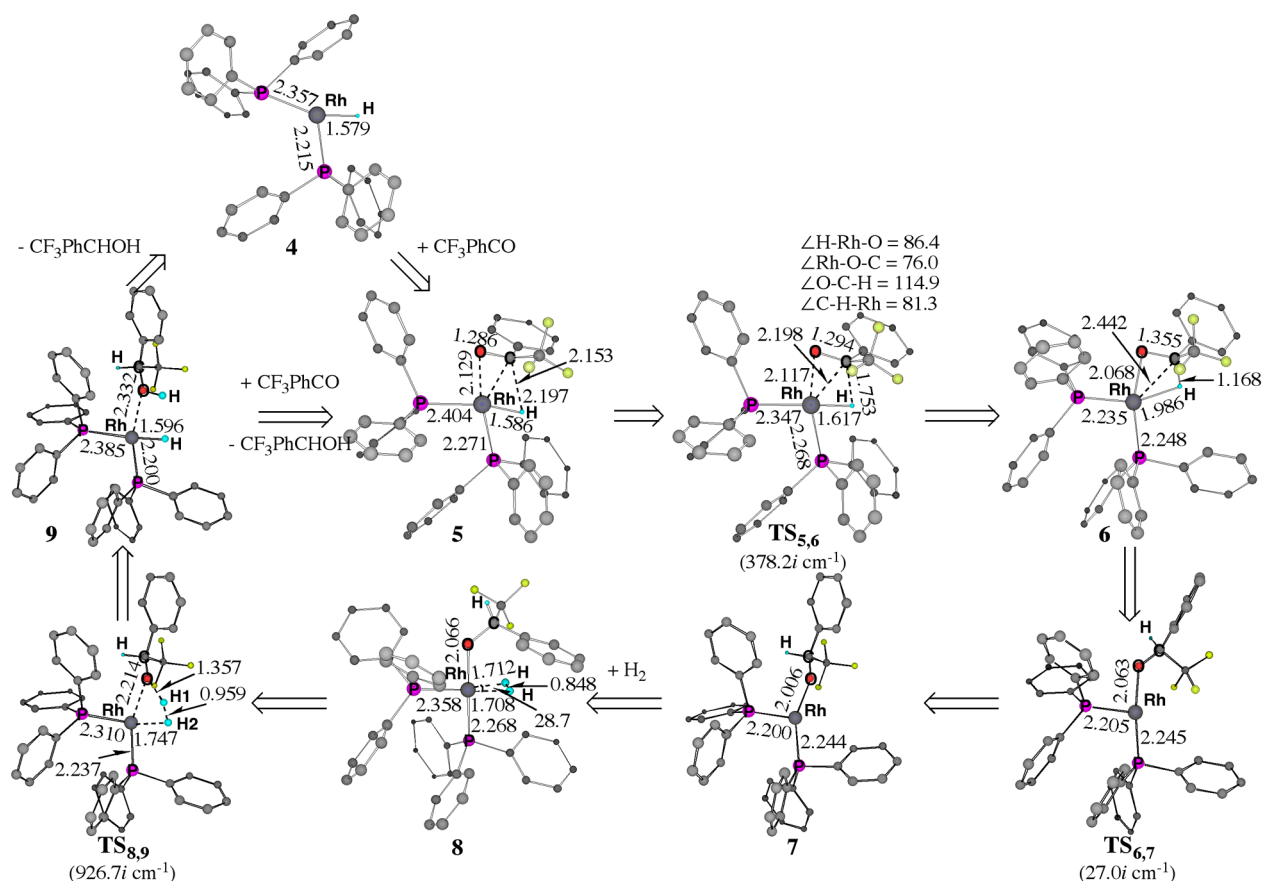


Figure 4. Geometry changes in the catalytic hydrogenation of CF_3PhCO by the Rh(I) hydride **4**. B3PW91/BS-1 level. Hydrogen atoms are omitted for clarity. Distances and angles are in Å and degrees, respectively.

slightly larger than that of CF_3PhCO , this CT is intrinsically small. Thus, it is reasonably concluded that the higher reactivity of CF_3PhCO , than those of $(\text{CH}_3)_2\text{CO}$ and Ph_2CO , arises from the electronic factor, i.e., the lower-lying $\text{C}=\text{O}$ π^* -antibonding MO of CF_3PhCO .

Catalytic Hydrogenation of 2,2,2-Trifluoroacetophenone by Ge(II) Hydride Compound **1.** For the catalytic hydrogenation, the next step is the reaction of **2** with a dihydrogen molecule. Two possible reaction pathways are investigated here: one is metathesis of a dihydrogen molecule with the Ge–O bond of **2** and the other is the oxidative addition of a dihydrogen molecule to the Ge center of **2** followed by reductive elimination. The metathesis occurs through a transition state $\text{TS}_{2,1-\text{H}_2}$, as shown in Figure 1. In $\text{TS}_{2,1-\text{H}_2}$, the Ge–O (2.292 Å) bond becomes considerably longer, while the H–H bond (0.883 Å) is somewhat elongated. The Ge–H distance (1.992 Å) is still longer than that of **1**, and the O–H distance (1.416 Å) is also much longer than in alcohol (0.965 Å). These geometrical features show that $\text{TS}_{2,1-\text{H}_2}$ has a distorted four-membered structure. The E_a and $\Delta G^{0\ddagger}$ values are 46.6 and 51.3 kcal/mol, respectively, indicating that this step is difficult. The reason of the difficulty will be discussed in detail in the latter section.

The oxidative addition occurs through a transition state $\text{TS}_{2,3}$ to afford a five-coordinate Ge dihydride **3**; see Figure S2. In **3**, the Ge center takes a trigonal bipyramidal structure, which is consistent with the hypervalent Ge species where the most negatively charged O and the next negatively charged N atom take positions on the pseudo- C_3 axis. However, this process is

endothermic; $\Delta E = 12.6$ kcal/mol and $\Delta G^0 = 17.2$ kcal/mol. The E_a and $\Delta G^{0\ddagger}$ values are also significantly large, 74.7 and 78.5 kcal/mol, respectively, indicating that this reaction is also difficult. This result is clearly different from the facile dihydrogen activation by carbene ($:\text{CR}_2$) which occurs with a moderate activation energy (25 kcal/mol) to afford a four-coordinate carbon compound.³⁹ The large activation energy of this oxidative addition arises from the absence of the empty valence orbital on the Ge atom of **2**; remember that carbene possesses both the doubly occupied lone-pair MO and the vacant p orbital which contribute to the CTs from carbene to dihydrogen and from dihydrogen to carbene. From **3**, one hydride migrates from the Ge center to the O atom through a transition state $\text{TS}_{3,1}$ to produce **1** and CF_3PhCHOH . This process also needs a very large activation energy; $E_a = 41.3$ and $\Delta G^{0\ddagger} = 36.7$ kcal/mol.

From these results, it should be concluded that the catalytic cycle for hydrogenation of CF_3PhCO cannot be constructed with **1**. We need to elucidate the reason why the catalytic hydrogenation of CF_3PhCO is difficult by **1**.

Catalytic Hydrogenation of Ketone by Rh(I) Hydride Complex **4.** $\text{RhH}(\text{PPh}_3)_3$ has been often employed in catalytic hydrogenation, racemization, and hydrogen-transfer reactions of ketone and alcohol.²² Though the hydrogenation of CO_2 with Rh(I) and Ru(II) hydride complexes has been theoretically investigated,^{40,41} that of ketone has not. Here, we investigated the hydrogenation reaction of CF_3PhCO by *cis*- $\text{Rh}(\text{PPh}_3)_2$ **4**; note that **4** was experimentally proposed as an active species.²² Because CH_3PhCO was employed in the

experiment, we also calculated the hydrogenation of CH_3PhCO with **4** to check if the catalytic hydrogenation certainly occurs; see Figures S3–S5. As shown in Figure 4, CF_3PhCO approaches the open-coordination site of **4** to afford an intermediate **5** with no barrier and significantly large exothermicity; $\Delta E = -35.8$ kcal/mol and $\Delta G^0 = -20.9$ kcal/mol. In **5**, CF_3PhCO coordinates with the Rh center through the $\text{C}=\text{O}$ double bond (1.286 Å) which becomes somewhat longer than in free CF_3PhCO (1.214 Å).

The next step is the insertion of the $\text{C}=\text{O}$ double bond of ketone into the Rh–H bond, which occurs through a transition state $\text{TS}_{5,6}$ to afford a Rh-alkoxide complex **6**. In $\text{TS}_{5,6}$, the hydride is approaching the carbonyl carbon, and simultaneously the carbonyl oxygen is approaching the Rh center; see the $\text{Rh}\cdots\text{O}$ (2.117 Å), $\text{Rh}\cdots\text{H}$ (1.617 Å), and $\text{Rh}\cdots\text{C}$ (2.198 Å) distances in Figure 4. In other words, the four-membered ring is less distorted in $\text{TS}_{5,6}$ than in $\text{TS}_{1,2}$; see the bond angles of $\text{TS}_{1,2}$ and $\text{TS}_{5,6}$ in Figures 1 and 4. This difference arises from the difference in valence orbital between the Rh and Ge centers; because the Rh center has an empty d orbital, it can form a bonding interaction between the Rh center and the carbonyl oxygen besides the interaction between the carbonyl carbon and the hydride in $\text{TS}_{5,6}$. But, the Ge center does not form such a bonding interaction between the Ge center and the carbonyl oxygen in $\text{TS}_{1,2}$ because of the fully occupied valence orbitals. The E_a and $\Delta G^{0\dagger}$ values are 5.9 and 6.8 kcal/mol, respectively, indicating that the ketone insertion reaction occurs much easier than that with **1**. The population analysis shows that the CT occurs from the d_{σ} and d_{xy} orbitals of the Rh center to the $\text{C}=\text{O}$ π^* -antibonding MO of CF_3PhCO , as shown in Figure 3b. The CT to the ketone moiety is similar between $\text{TS}_{5,6}$ (0.51e) and $\text{TS}_{1,2}$ (0.53e). However, the CT from the ketone to the Ge moiety is negligibly small in $\text{TS}_{1,2}$ (0.01e). On the other hand, the CT from the ketone to the Rh moiety somewhat contributes to $\text{TS}_{5,6}$ (0.09e), which is consistent with the presences of typical donation and back-donation interactions in a transition-metal complex. In **6**, the agostic interaction is formed between the C–H bond and the Rh center; see the C–H distance of 1.168 Å and the Rh–H distance of 1.986 Å. Then, this interaction is broken by the rotation of the alkoxide moiety to afford the Rh-alkoxide species **7** with the moderate E_a and $\Delta G^{0\dagger}$ values of 5.7 and 5.7 kcal/mol, respectively.

A dihydrogen molecule approaches the open-coordination site of **7** without any barrier to produce an η^2 -dihydrogen complex **8** with ΔE and ΔG^0 values of -5.1 and 1.4 kcal/mol, respectively, as shown in Figures 4 and 2b, where the $\text{Rh}\cdots\text{H}$ distances are equivalent (1.712 Å and 1.708 Å) with the H–H distance of 0.848 Å. From **8**, two pathways are possible. One is metathesis-like heterolytic H–H bond cleavage of a dihydrogen molecule with the Rh–O bond. The H–H and Rh–O bond cleavages occur via a four-membered transition state $\text{TS}_{8,9}$, concomitantly with the O–H and Rh–H bond formations, where E_a and $\Delta G^{0\dagger}$ values are 16.2 and 16.2 kcal/mol, respectively. In $\text{TS}_{8,9}$, the H1 is positively charged (+0.29), but the H2 is negatively charged (−0.05), indicating that this reaction is understood to be a heterolytic σ -bond cleavage to afford an alcohol complex $\text{RhH}(\text{PPh}_3)_2(\text{PhFH}_3\text{CHOH})$ **9**; see $\text{TS}_{8,9}$ in Figure 4 for H1 and H2. Another is oxidative addition of a dihydrogen molecule to the Rh center followed by reductive elimination to produce CF_3PhCHOH and **4**. The oxidative addition occurs through a transition state $\text{TS}_{8,10}$ to afford an intermediate **10** with the small ΔE and ΔG^0 values of

0.7 and -1.5 kcal/mol, respectively; see Figure S6. In **10**, two hydrides and the alkoxide oxygen independently coordinate with the Rh center, indicating that **10** is a square pyramidal Rh(III) complex. Then, the reductive elimination occurs between the hydride at the axial position and the alkoxide oxygen through a three-membered transition state $\text{TS}_{10,9}$ to afford **9**. The E_a and $\Delta G^{0\dagger}$ values are 15.5 and 15.6 kcal/mol, respectively. The final step is either the formation of the active species **4** through alcohol elimination from the Rh center or the formation of the intermediate **5** through substitution of ketone for alcohol.

From these results, it is concluded that the oxidative addition pathway is slightly more favorable than the metathesis-like H–H σ -bond cleavage pathway and that the hydrogenation of ketone by **4** occurs much easier than by **1**.

Comparison of Catalytic Cycle between Ge(II) Hydride and Rh(I) Hydride Compounds. It is considerably important to elucidate the reason why a dihydrogen molecule easily reacts with the Rh(I) alkoxide **7** but does not with the Ge(II) alkoxide **2**. In this process, the M–O and H–H bonds (M = Rh or Ge) are broken, and the M–H and O–H bonds are formed. As shown in Figure 5, the Rh–O and Ge–O bond energies are

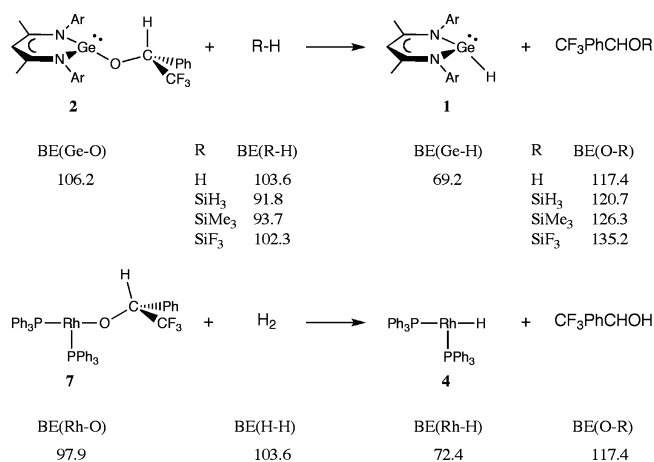


Figure 5. Calculated bond energies (BE; kcal/mol) concerning the reactions of **2** and **7** with H_2 and SiR_3H at the SCS-MP2/BS-2//B3PW91/BS-1 level.⁴²

evaluated to be 97.9 and 106.2 kcal/mol in **7** and **2**, respectively. The Rh–H and Ge–H bond energies are 72.4 and 69.2 kcal/mol in **4** and **1**.⁴² In the hydrogenation by **1**, the stronger Ge–O bond is broken, but the weaker Ge–H bond is formed. In the hydrogenation by **4**, on the other hand, the weaker Rh–O bond is broken, and the stronger Rh–H bond is formed. These results indicate that the strong Ge–O bond of **2** is one of the reasons for the difficulty in constructing a catalytic cycle with **1**.⁴³

A comparison of energy changes between the catalytic cycles by **1** and **4** also exhibits interesting differences (Figure 2). In the case of **4**, neither a significantly large energy increase nor decrease is observed, which is one of the typical features of the catalytic reaction by a transition-metal complex. In the case of **1**, on the other hand, a significantly large energy decrease occurs in the process $\text{TS}_{1,2} \rightarrow \textbf{2}$, but a large energy increase occurs in the process $\textbf{2} \rightarrow \textbf{1} + \text{CF}_3\text{PhCHOH}$. This feature also arises from the very strong Ge–O bond, because the former process involves the Ge–O bond formation, but the latter one does the Ge–O bond cleavage.

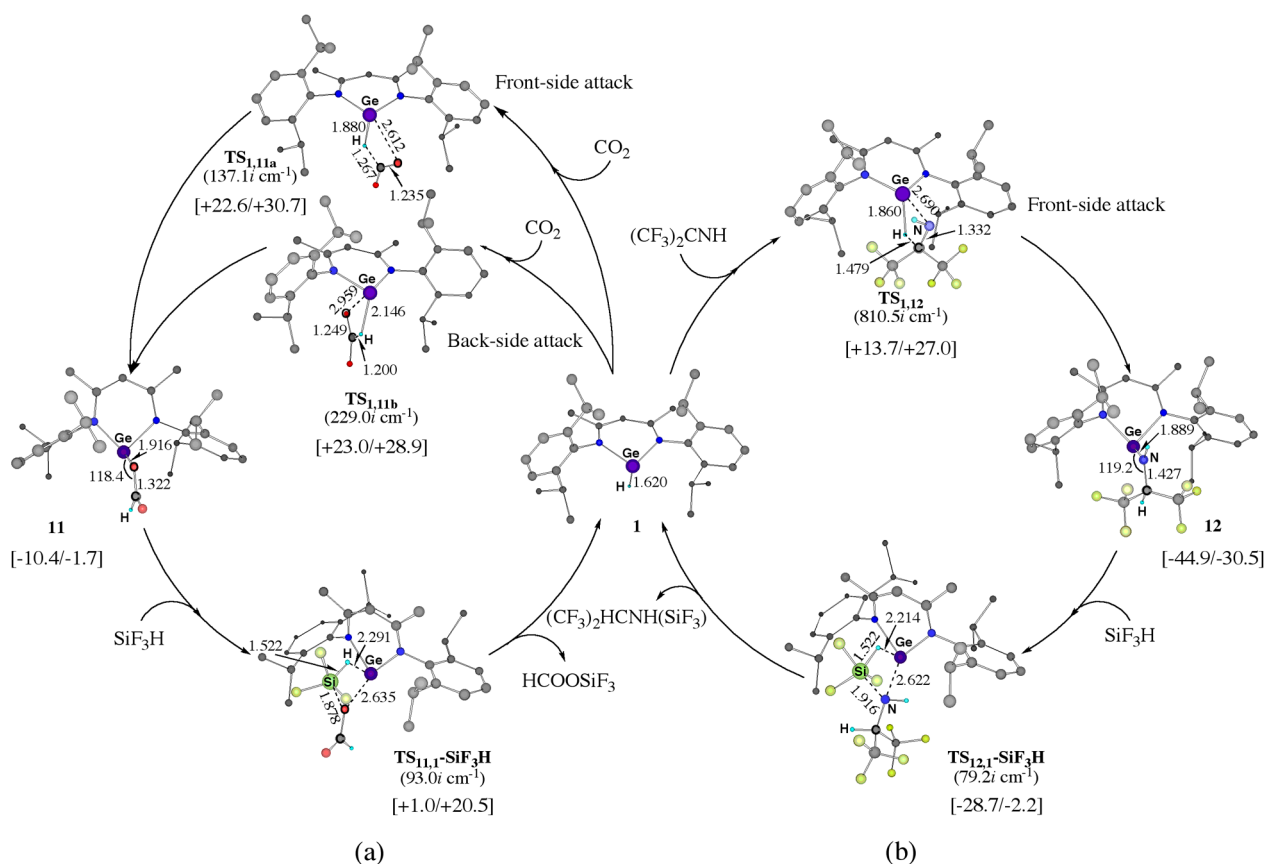


Figure 6. Geometry and energy changes in hydrosilylation of (a) CO_2 and (b) imine by the Ge(II) hydride **1**. B3PW91/BS-1 level. Hydrogen atoms are omitted for clarity. Distances and angles are in Å and degrees, respectively.

Prediction of Full Catalytic Cycle for Ketone Transformation by Ge(II) Hydride Compound **1.** To construct a full catalytic cycle with **1**, the Ge–O bond must become weaker, and the Ge–H bond must become stronger. Despite various examinations of substituent effects on these two bond energies, we could not find a good candidate to satisfy these two requests. Another way is to stabilize the transition state and the product by using a different reagent. In the hydrogenation reaction, **1** is regenerated with the formation of alcohol. If silane (SiR_3H) is employed instead of a dihydrogen molecule, **1** is reproduced with the formation of silyl ether. The Si–O bond is strong, as is well-known. Hence, one can expect that the product becomes more stable when silane is employed. Note that silyl ether easily undergoes hydrolysis to afford alcohol; in other words, the silylation of ketone is equivalent to the hydrogenation. Thus, we employed here silane (SiH_4), trimethylsilane (SiMe_3H), and trifluorosilane (SiF_3H). This hydrosilylation reaction occurs in one step via a four-membered metathesis-like transition state; see Figure 1 for a transition state $\text{TS}_{2,1}\text{-SiF}_3\text{H}$ and Figure S7 for $\text{TS}_{2,1}\text{-SiH}_4$ and $\text{TS}_{2,1}\text{-SiMe}_3\text{H}$. When SiH_4 is employed, the E_a (45.0 kcal/mol) and $\Delta G^{0\ddagger}$ (53.2 kcal/mol) values are not very different from those of the hydrogenation (46.6 and 51.3 kcal/mol, respectively). However, the ΔE and ΔG^0 values (–33.1 and –24.6 kcal/mol, respectively) become more negative than those (–15.9 and –10.0 kcal/mol) of the hydrogenation, as expected. When SiMe_3H is employed, the E_a and $\Delta G^{0\ddagger}$ values decrease to 37.2 and 51.5 kcal/mol but are still large. A drastic change is observed when SiF_3H is employed. The E_a and $\Delta G^{0\ddagger}$ values are

13.3 and 23.1 kcal/mol, respectively, suggesting that this reaction easily occurs, as shown in Figure 2a.

In this hydrosilylation reaction, the Ge–O and Si–H bonds are broken, and the Si–O and Ge–H bonds are formed. We evaluated these bond energies,⁴² as shown in Figure 5. The Si–H bond energy of silane increases in the order of $\text{SiH}_3\text{–H}$ (91.8 kcal/mol) < $\text{SiMe}_3\text{–H}$ (93.7 kcal/mol) < $\text{SiF}_3\text{–H}$ (102.3 kcal/mol), and the Si–O bond energy of silyl ether increases in the order of $\text{CF}_3\text{PhCHO-SiH}_3$ (120.7 kcal/mol) < $\text{CF}_3\text{PhCHO-SiMe}_3$ (126.3 kcal/mol) < $\text{CF}_3\text{PhCHO-SiF}_3$ (135.2 kcal/mol). Though the Si–H bond of $\text{SiF}_3\text{–H}$ is stronger than in the others, the Si–O bond of $\text{CF}_3\text{PhCHO-SiF}_3$ becomes much more stronger than in the others. As a result, the maximum energy gain is obtained with SiF_3H .

Because the reaction of **2** with silane is important here, we examined its transition state $\text{TS}_{2,1}\text{-SiF}_3\text{H}$. In this transition state, the Si center takes a trigonal bipyramidal five-coordinate structure which indicates the hypervalency of the Si center. The CT occurs from the lone-pair MO of the O atom of the Ge-alkoxide moiety to the vacant p orbital of the hypervalent Si center and from the Si–H σ -bonding MO to the 5p orbital of the Ge center, as shown in Figure 3c. The lone-pair MO of the Ge center contributes little to this reaction too. Interestingly, the former CT is the largest in the case of SiF_3H and becomes smaller in the order of SiF_3H (0.13e) > SiH_4 (0.07e) ~ SiMe_3H (0.07e), where in parentheses is the electron population on the vacant p orbital of the distorted silane.⁴⁴ This is because the vacant p orbital energy of the distorted silanes becomes higher in the order of SiF_3H (+1.08 eV) < SiH_4 (+2.57 eV) < SiMe_3H (+3.31 eV). The transition state is also stabilized by the

electrostatic interaction between the positively charged Si atom and the negatively charged O atom; see the increasing order of the Si atomic charge of the distorted silanes, SiH_4 (+0.61) < SiMe_3H (+1.34) < SiF_3H (+2.06). This is the reason of the shorter $\text{Si}\cdots\text{O}$ distance in $\text{TS}_{2,1}\text{-SiF}_3\text{H}$ than in $\text{TS}_{2,1}\text{-SiH}_4$ and $\text{TS}_{2,1}\text{-SiMe}_3\text{H}$. Both of the large CT and the large electrostatic interactions lead to the higher reactivity of SiF_3H . It is shown that this catalytic hydrosilylation of CF_3PhCO by **1** is more accelerated in polar solvent due to the highly polar electronic structure of the transition state; see page S3 in the Supporting Information for the details.

In conclusion, we wish to propose a theoretical prediction that a catalytic cycle of the hydrosilylation of ketone can be constructed with a combination of the Ge(II) hydride compound **1** and SiF_3H . The rate-determining step in the Gibbs energy is the ketone insertion into the Ge–H bond of **1**.

Prediction of Catalytic Cycle for Hydrosilylation of Carbon Dioxide by Ge(II) Hydride Compound 1. The polarized $\text{C}=\text{O}$ double bond of ketone reacts with **1**. The $\text{C}=\text{O}$ double bond of CO_2 is also polarized, suggesting the possibility that one can construct the catalytic cycle of the hydrosilylation of CO_2 with **1**. As experimentally reported,^{16–18} **1** actually reacts with CO_2 to afford a Ge(II) formate **11**, as shown in Scheme 2a. However, as mentioned above, the catalytic cycle has not been constructed yet. We investigated whether the catalytic hydrosilylation of CO_2 by **1** can be performed with SiF_3H or not. CO_2 approaches the Ge–H bond in the less congested front-side of **1**, and the CO_2 insertion occurs in one step through a four-membered transition state $\text{TS}_{1,11a}$ to afford a Ge(II) formate **11**, as shown in Figure 6a. In $\text{TS}_{1,11a}$, the $\text{C}\cdots\text{H}$ (1.267 Å) distance is much shorter than in $\text{TS}_{1,2}$ (1.434 Å), whereas the $\text{Ge}\cdots\text{O}$ distance is little different; 2.612 Å in $\text{TS}_{1,11a}$ and 2.623 Å in $\text{TS}_{1,2}$. This means that $\text{TS}_{1,11a}$ is more product-like than $\text{TS}_{1,2}$, which is consistent with the much larger E_a and $\Delta G^{0\ddagger}$ values (22.6 and 30.7 kcal/mol, respectively) for the CO_2 insertion than those for the CF_3PhCO insertion (10.9 and 24.8 kcal/mol). The larger activation energy in the CO_2 insertion is explained by its higher-lying $\text{C}=\text{O}$ π^* -antibonding MO (+5.28 eV); remember that the $\text{C}=\text{O}$ π^* -antibonding MO of CF_3PhCO is +1.25 eV. Actually, the electron population (1.54e) of the Ge–H σ -bonding MO in $\text{TS}_{1,11a}$ is slightly larger than that (1.52 e) in $\text{TS}_{1,2}$, suggesting that the CT occurs smaller in $\text{TS}_{1,11a}$ than in $\text{TS}_{1,2}$. The ΔE and ΔG^0 values (–10.4 and –1.7 kcal/mol) are less exothermic than those of the CF_3PhCO insertion.

We wish to briefly discuss several other possible reaction pathways. In one pathway, CO_2 is inserted into the Ge–H bond from the more congested backside of **1** to afford the Ge(II) formate **11** through a transition state $\text{TS}_{1,11b}$, as shown in Figure 6a. This insertion occurs with E_a and $\Delta G^{0\ddagger}$ values of 23.0 and 28.9 kcal/mol, respectively, similar to those of the former insertion, suggesting that both insertion pathways are possible. The insertion of ketone does not occur in this congested side, because ketone is much more bulky than CO_2 ; see Figure S8a. In the reaction between CO_2 and amidodigermene, CO_2 bounds with the Ge atom first.¹⁰ Considering this reaction, we examined if CO_2 coordinates with the Ge center through the C atom, the O atom, or the $\text{C}=\text{O}$ double bond. However, these coordinations are difficult, indicating that the coordination of CO_2 with the Ge center does not occur prior to the insertion reaction; see Figure S9c–e. We also investigated the CO_2 insertion in the different regioselectivity to afford a Ge–COOH species. However, we could not locate

the transition state because this insertion is very difficult, as reported previously;⁴⁵ see Figure S9b. This is interpreted in terms of the poor orbital overlap and the unfavorable electrostatic interaction, as follows: The positively charged carbon atom and the negatively charged oxygen atom of CO_2 approach the positively charged Ge(II) center and the negatively charged hydride, respectively, indicating that the electrostatic interaction is not favorable. Also, the π^* -antibonding MO of CO_2 less overlaps with the HOMO of the Ge(II)–H moiety in this insertion than in the normal insertion, because the p orbital lobe of the C atom is much larger than that of the O atom in the π^* -antibonding MO; see Figure S10. Based on the above results, it is likely to conclude that the CO_2 insertion reactions via $\text{TS}_{1,11a}$ and $\text{TS}_{1,11b}$ are possible, but the insertion with the reverse regioselectivity does not occur.

The second step is the reaction of **11** with SiF_3H . This reaction occurs through a four-membered metathesis-like transition state $\text{TS}_{11,1}\text{-SiF}_3\text{H}$ which is similar to $\text{TS}_{2,1}\text{-SiF}_3\text{H}$ (Figure 6a). The $\text{Ge}\cdots\text{O}$ distance (2.635 Å) in $\text{TS}_{11,1}\text{-SiF}_3\text{H}$ is much longer than in $\text{TS}_{2,1}\text{-SiF}_3\text{H}$ (2.400 Å), whereas the other bond distances, such as the $\text{Ge}\cdots\text{H}$, $\text{Si}\cdots\text{H}$, and $\text{Si}\cdots\text{O}$, are not different so much. In $\text{TS}_{11,1}\text{-SiF}_3\text{H}$, the CT occurs from the lone-pair MO of the O atom of the Ge–OCOH moiety to the vacant p orbital of the silane moiety like $\text{TS}_{2,1}\text{-SiF}_3\text{H}$, where the electron population (0.24e) in the p orbital is almost same as that (0.25e) of $\text{TS}_{2,1}\text{-SiF}_3\text{H}$.⁴⁶ These results are consistent with the fact that the E_a and $\Delta G^{0\ddagger}$ values (11.4 and 22.2 kcal/mol, respectively) are close to those of **2** (13.3 and 23.1 kcal/mol).

We also performed additional calculations about the oxidative addition of SiF_3H to the Ge center of **11** to afford a five-coordinate Ge hydride silyl species **13**. This reaction needs a very large activation energy ($E_a = 39.4$ and $\Delta G^{0\ddagger} = 58.3$ kcal/mol, respectively) like the oxidative addition of a dihydrogen molecule to **2**; see Figure S11. Hence, the regeneration of **1** occurs through the metathesis-like pathway like in the hydrosilylation of CF_3PhCO .

Based on the above results, it should be concluded that the catalytic hydrosilylation of CO_2 can be also performed with **1** to afford a silylformate. The rate-determining step of this catalytic hydrosilylation of CO_2 is the CO_2 insertion process into the Ge–H bond of **1**.

Prediction of Catalytic Cycle for Hydrosilylation of Imine by Ge(II) Hydride Compound 1. Because imine has a polarized $\text{C}=\text{N}$ double bond which is similar to a $\text{C}=\text{O}$ double bond of ketone and carbon dioxide, one can expect that the $\text{C}=\text{N}$ double bond is inserted into the Ge–H bond. However, no experiment of the reaction of imine with **1** has been reported. We investigated the reactions of several imines and found that the $\text{C}=\text{N}$ double bond can be inserted into the Ge–H bond, when R and R' are an electron-withdrawing group, such as CF_3 . This is because the $\text{C}=\text{N}$ π^* -antibonding MO energy becomes lower in bis(trifluoromethyl)imine $(\text{CF}_3)_2\text{C}=\text{NH}$.⁴⁷ The insertion of the $\text{C}=\text{N}$ double bond of $(\text{CF}_3)_2\text{C}=\text{NH}$ into the Ge–H bond occurs in the less congested front-side of **1** through a four-membered transition state $\text{TS}_{1,12}$, like $\text{TS}_{1,2}$ and $\text{TS}_{1,11a}$, as shown in Figure 6b. In $\text{TS}_{1,12}$, the $\text{C}\cdots\text{H}$ distance (1.479 Å) is longer than in $\text{TS}_{1,11}$ for the CO_2 insertion but close to those in $\text{TS}_{1,2}$ (1.434 Å), $\text{TS}_{1,2b}$ (1.481 Å), and $\text{TS}_{1,2c}$ (1.457 Å) for ketone insertion. The E_a and $\Delta G^{0\ddagger}$ values are 13.7 and 27.0 kcal/mol, respectively, which are somewhat larger than those of the CF_3PhCO insertion (10.9 and 24.8 kcal/mol) but smaller than the CO_2 insertion

(22.6 and 30.7 kcal/mol). These results suggest the higher reactivity of imine than CO_2 . This higher reactivity of $(\text{CF}_3)_2\text{C}=\text{NH}$ is consistent with the electron distribution in $\text{TS}_{1,12}$, as follows: The electron population of the Ge–H σ -bonding MO is smaller in $\text{TS}_{1,12}$ (1.48e) than in $\text{TS}_{1,2}$ (1.52e) and $\text{TS}_{1,11a}$ (1.54e), indicating that the CT occurs more in $\text{TS}_{1,12}$ than in $\text{TS}_{1,2}$ and $\text{TS}_{1,11a}$. The C=N π^* -antibonding MO energy of $(\text{CF}_3)_2\text{C}=\text{NH}$ is calculated to be +2.21 eV, which is much higher than that of CF_3PhCO (+1.25 eV) and Ph_2CO (+1.76 eV) but significantly lower than those of $(\text{CH}_3)_2\text{CO}$ (+3.84 eV) and CO_2 (+5.28 eV). Hence, it is concluded that the higher reactivity of $(\text{CF}_3)_2\text{C}=\text{NH}$ arises from the lower-lying π^* -antibonding MO energy of the C=N double bond. The ΔE and ΔG^0 values are –44.9 and –30.5 kcal/mol, respectively. This reaction is more exothermic than the CO_2 insertion but similar to the CF_3PhCO insertion.

We examined if the insertion of $(\text{CF}_3)_2\text{C}=\text{NH}$ occurs in the more congested backside, as found in $\text{TS}_{1,11b}$. However, we could not locate the transition state due to the more congested structure like the ketone insertion; see Figure S8b. We also investigated the insertion of $(\text{CF}_3)_2\text{C}=\text{NH}$ into the Ge–H bond in the different regioselectivity and found that it is difficult like the CO_2 insertion. This is because the unfavorable electrostatic interaction and unfavorable orbital overlap; see Figures S9f and S10.

The next step is the reaction of **12** with SiF_3H . This reaction occurs through a four-membered transition state $\text{TS}_{12,1}-\text{SiF}_3\text{H}$ (Figure 6b) to afford silylamine $(\text{CF}_3)_2\text{HCNH}(\text{SiF}_3)$. In $\text{TS}_{12,1}-\text{SiF}_3\text{H}$, the CT occurs from the lone-pair MO of the N atom to the vacant p orbital of the distorted SiF_3H , too. The electron population (0.27e) of the vacant p orbital is slightly larger than in $\text{TS}_{2,1}-\text{SiF}_3\text{H}$ (0.25e) and $\text{TS}_{11,1}-\text{SiF}_3\text{H}$ (0.24e). However, the E_a and $\Delta G^{0\ddagger}$ values (16.2 and 28.3 kcal/mol, respectively) are somewhat larger than in $\text{TS}_{2,1}-\text{SiF}_3\text{H}$ (13.3 and 23.1 kcal/mol) and $\text{TS}_{11,1}-\text{SiF}_3\text{H}$ (11.4 and 22.2 kcal/mol). Though the reason is not clear at this moment, one plausible reason is that the N atom of **12** has only one lone-pair orbital to interact with silane, but the O atom has two lone-pair orbitals in **2** and **11**.⁴⁸

Besides the metathesis, we examined the oxidative addition of SiF_3H to the Ge center. This oxidative addition occurs through the transition state $\text{TS}_{12,14}$ to afford a five-coordinate Ge dihydride **14**, but it is difficult ($E_a = 37.2$ and $\Delta G^{0\ddagger} = 50.9$ kcal/mol, respectively); see Figure S11.

From these results, it is theoretically concluded that the catalytic hydrosilylations of imine can be performed with **1** to afford a silylamine, in which the C=N double bond is inserted into the Ge–H bond of **1** via $\text{TS}_{1,12}$ followed by metathesis with SiF_3H . The rate-determining step of this catalytic hydrosilylation of imine is the reaction of **12** with SiF_3H .

CONCLUSIONS

The catalytic conversion of ketone with the Ge(II) hydride compound **1** was theoretically investigated with the DFT and SCS-MP2 methods. CF_3PhCO easily reacts with **1** to afford the corresponding Ge(II) alkoxide **2**. This reaction occurs through the CT from the Ge–H σ -bonding MO of **1** to the C=O π^* -antibonding MO of CF_3PhCO . The lone-pair MO of **1** contributes little to this reaction. The high reactivity of CF_3PhCO arises from the lower-lying C=O π^* -antibonding MO energy; because its orbital energy is much lower in CF_3PhCO than in $(\text{CH}_3)_2\text{CO}$ and Ph_2CO . Though **2** is easily formed from **1** and CF_3PhCO , our calculations indicate that the hydrogenation of **2** with a dihydrogen molecule is difficult, and

hence it is not easy to construct a full catalytic cycle for hydrogenation of ketone. On the other hand, theoretical calculations show that the catalytic hydrogenation of ketone by the Rh(I) hydride complex **4** easily occurs without large energy barrier, as expected.

Detailed comparison of the catalytic cycle between **1** and **4** discloses that the strong Ge–O bond of the Ge(II) alkoxide **2** is one of the important reasons of difficulty in constructing a catalytic cycle with **1**. This finding suggests to us an idea that a full catalytic cycle can be constructed by using some reagent which leads to the formation of a product stable enough to compensate the Ge–O bond cleavage. One such reagent is silane because the Si–O bond is strong, as is well-known. We examined three silanes and found that SiF_3H is a good reagent to construct the catalytic cycle. In the transition state of the reaction between **2** and SiF_3H , the Si center takes a hypervalent five-coordinate structure. The CT strongly occurs from the lone-pair orbital of the alkoxide oxygen to the vacant p orbital of the hypervalent Si center. In addition, the electrostatic interaction between the positively charged Si atom and the negatively charged O atom is responsible for the small activation energy. As a result, the reaction of **2** with SiF_3H easily occurs unlike the reaction of **2** with a hydrogen molecule. From these results, we wish to propose here that a full catalytic cycle for hydrosilylation of ketone by **1** can be constructed with SiF_3H .

The catalytic cycles of hydrosilylations of CO_2 and imine by **1** can be predicted with SiF_3H , similarly. The C=O double bond of CO_2 and the C=N double bond of imine can be inserted into the Ge–H bond of **1** to afford a Ge(II) formate and Ge(II) amino compounds, respectively. Then, these intermediates easily react with SiF_3H to regenerate **1** with the moderate activation barrier. The electronic processes of these reactions are similar to that of the reaction with Ge(II) alkoxide compound **2**.

We believe that this theoretical prediction of a full catalytic cycle by a heavier main-group element compound is useful to open a new area of main-group element chemistry.

ASSOCIATED CONTENT

Supporting Information

Details of correction of the translational entropy in solvent and populations analysis based on the MOs of fragments; solvent effect on hydrosilylation of CF_3PhCO with **1** and silanes; optimized structures of $\text{TS}_{1,2b}$, **2b**, $\text{TS}_{1,2c}$, **2c**, $\text{TS}_{2,3}$, **3**, $\text{TS}_{3,1'}$, **5'**, $\text{TS}_{5,6'}$, **6'**, $\text{TS}_{6,7'}$, **7'**, **8'**, $\text{TS}_{8,9'}$, **9'**, $\text{TS}_{8,10'}$, **10'**, $\text{TS}_{10,9'}$, $\text{TS}_{8,10}$, **10**, $\text{TS}_{10,9}$, $\text{TS}_{2,1}-\text{SiH}_4$, $\text{TS}_{2,1}-\text{SiMe}_3\text{H}$, $\text{TS}_{11,13}$, **13**, $\text{TS}_{12,14}$, and **14**; potential and Gibbs energy changes in the hydrogenation of CH_3PhCO by the Rh(I) hydride **4**; assumed structures of ketone and imine insertion into the different side of the Ge–H bond of **1**; potential energy curves for interaction of ketone, CO_2 , imine with **1** and dimerization of **1**; NBO charge and frontier orbitals of CF_3PhCO , CO_2 , $(\text{CF}_3)_2\text{CHN}$, and **1**; comparison of optimized structures of **1** and **2** with the experimental values; energy changes of model systems with various computational method up to MP4(SDQ) and CCSD-(T) levels; complete ref 38; and the Cartesian coordinate and total energies of all the optimized structures in this work. This material is available free of charge via the Internet at <http://pubs.acs.org>.

■ AUTHOR INFORMATION

Corresponding Author

sakaki.shigeyoshi.47e@st.kyoto-u.ac.jp

Notes

The authors declare no competing financial interest.

■ ACKNOWLEDGMENTS

This work is financially supported by the Ministry of Education, Culture, Science, Sport, and Technology through a Grant-in-Aid of Specially Promoted Science and Technology (no. 22000009). We wish to thank the computer center of Institute for Molecular Science (IMS, Okazaki, Japan) for kind use of computers.

■ REFERENCES

- (1) See a review for heavier ethylenes and acetylenes and references therein; Fischer, R. C.; Power, P. P. *Chem. Rev.* **2010**, *110*, 3877.
- (2) (a) Wakita, K.; Tokitoh, N.; Okazaki, R.; Nagase, S. *Angew. Chem.* **2000**, *112*, 648; *Angew. Chem., Int. Ed.* **2000**, *39*, 634. (b) Nakata, N.; Takeda, N.; Tokitoh, N. *J. Am. Chem. Soc.* **2002**, *124*, 6914.
- (3) Li, L.; Fukawa, T.; Matsuo, T.; Hashizume, D.; Fueno, H.; Tanaka, K.; Tamao, K. *Nat. Chem.* **2012**, *4*, 361.
- (4) See a review for heavier carbenes and references therein; Mizuhata, Y.; Sasamori, T.; Tokitoh, N. *Chem. Rev.* **2009**, *109*, 3479.
- (5) (a) Spikes, G. H.; Fetting, J. C.; Power, P. P. *J. Am. Chem. Soc.* **2005**, *127*, 12232. (b) Peng, Y.; Brynda, M.; Ellis, B. D.; Fetting, J. C.; Rivard, E.; Power, P. P. *Chem. Commun.* **2008**, 6042.
- (6) Peng, Y.; Guo, J. D.; Ellis, B. D.; Zhu, Z.; Fetting, J. C.; Nagase, S.; Power, P. P. *J. Am. Chem. Soc.* **2009**, *131*, 16272.
- (7) Li, J.; Schenk, C.; Goedecke, C.; Frenking, G.; Jones, C. *J. Am. Chem. Soc.* **2011**, *133*, 18622.
- (8) Yao, S.; Xiong, Y.; Driess, M. *Organometallics* **2011**, *30*, 1748.
- (9) Wang, X.; Zhu, Z.; Peng, Y.; Lei, H.; Fetting, J. C.; Power, P. P. *J. Am. Chem. Soc.* **2009**, *131*, 6912.
- (10) Li, J.; Hermann, M.; Frenking, G.; Jones, C. *Angew. Chem.* **2012**, *124*, 8739; *Angew. Chem., Int. Ed.* **2012**, *51*, 8611.
- (11) (a) Cui, C.; Olmstead, M. M.; Fetting, J. C.; Spikes, G. H.; Power, P. P. *J. Am. Chem. Soc.* **2005**, *127*, 17530. (b) Kinjo, R.; Ichinohe, M.; Sekiguchi, A.; Takagi, N.; Sumimoto, M.; Nagase, S. *J. Am. Chem. Soc.* **2007**, *129*, 7766. (c) Peng, Y.; Ellis, B. D.; Wang, X.; Power, P. P. *Science* **2009**, *325*, 1668.
- (12) Cui, C.; Olmstead, M. M.; Fetting, J. C.; Spikes, G. H.; Power, P. P. *J. Am. Chem. Soc.* **2005**, *127*, 17530.
- (13) (a) Summerscales, O. T.; Fetting, J. C.; Power, P. P. *J. Am. Chem. Soc.* **2012**, *133*, 11960. (b) Summerscales, O. T.; Caputo, C. A.; Knapp, C. E.; Fetting, J. C.; Power, P. P. *J. Am. Chem. Soc.* **2012**, *134*, 14595. (c) Brown, Z. D.; Vasko, P.; Fetting, J. C.; Tuononen, H. M.; Power, P. P. *J. Am. Chem. Soc.* **2012**, *134*, 4045.
- (14) (a) Power, P. P. *Nature* **2010**, *463*, 171. (b) Power, P. P. *Acc. Chem. Res.* **2011**, *44*, 627. (c) Martin, D.; Soleilhavoup, M.; Bertrand, G. *Chem. Sci.* **2011**, *2*, 389.
- (15) Pineda, L. W.; Jancik, V.; Starke, K.; Oswald, R. B.; Roesky, H. W. *Angew. Chem.* **2006**, *118*, 2664; *Angew. Chem., Int. Ed.* **2006**, *45*, 2602.
- (16) Mandal, S. K.; Roesky, H. W. *Acc. Chem. Res.* **2012**, *45*, 298.
- (17) Jana, A.; Ghoshal, D.; Roesky, H. W.; Objartel, I.; Schwab, G.; Stalke, D. *J. Am. Chem. Soc.* **2009**, *131*, 1288.
- (18) Jana, A.; Tavčar, G.; Roesky, H. W.; John, M. *Dalton Trans.* **2010**, *39*, 9487.
- (19) Jana, A.; Roesky, H. W.; Schulzke, C. *Dalton Trans.* **2010**, *39*, 132.
- (20) Choong, S. L.; Woodul, W. D.; Schenk, C.; Stasch, A.; Richards, A. F.; Jones, C. *Organometallics* **2011**, *30*, 5543.
- (21) Jana, A.; Sen, S. S.; Roesky, H. W.; Schulzke, C.; Dutta, S.; Pati, S. K. *Angew. Chem.* **2009**, *121*, 4310; *Angew. Chem., Int. Ed.* **2009**, *48*, 4246.
- (22) Pàmies, O.; Bäckvall, J. E. *Chem.—Eur. J.* **2001**, *7*, 5052.
- (23) Clapham, S. E.; Hadzovic, A.; Morris, R. H. *Coord. Chem. Rev.* **2004**, *248*, 2201.
- (24) Brown, Z. D.; Guo, J. D.; Nagase, S.; Power, P. P. *Organometallics* **2012**, *31*, 3768.
- (25) Zhao, L.; Huang, F.; Lu, G.; Wang, Z. X.; Schleyer, P. v. R. *J. Am. Chem. Soc.* **2012**, *134*, 8856.
- (26) Caputo, C. A.; Koivisto, J.; Moilanen, J.; Boynton, J. N.; Tuononen, H. M.; Power, P. P. *J. Am. Chem. Soc.* **2013**, *135*, 1952.
- (27) Eichler, B. E.; Power, P. P. *J. Am. Chem. Soc.* **2000**, *122*, 8785.
- (28) (a) Becke, A. D. *Phys. Rev. A* **1988**, *38*, 3098. (b) Becke, A. D. *J. Chem. Phys.* **1993**, *98*, 5648.
- (29) Perdew, J. P.; Wang, Y. *Phys. Rev. B* **1992**, *45*, 13244.
- (30) Wadt, W. R.; Hay, P. J. *J. Chem. Phys.* **1985**, *82*, 299.
- (31) (a) Hehre, W. J.; Ditchfield, R.; Pople, J. A. *J. Chem. Phys.* **1972**, *56*, 2257. (b) Hariharan, P. C.; Pople, J. A. *Theor. Chim. Acta* **1973**, *28*, 213. (c) Francl, M. M.; Pietro, W. J.; Hehre, W. J.; Binkley, J. S.; Gordon, M. S.; DeFrees, D. J.; Pople, J. A. *J. Chem. Phys.* **1982**, *77*, 3654.
- (32) Martin, J. M. L.; Sundermann, A. *J. Chem. Phys.* **2001**, *114*, 3408.
- (33) (a) Andrae, D.; Haeussermann, U.; Dolg, M.; Stoll, H.; Preuss, H. *J. Theor. Chim. Acta* **1990**, *77*, 123. (b) Bergner, A.; Dolg, M.; Kuechle, W.; Stoll, H.; Preuss, H. *Mol. Phys.* **1993**, *80*, 1431.
- (34) Ehlers, A. W.; Böhme, M.; Dapprich, S.; Gobbi, A.; Höllwarth, A.; Jonas, V.; Köhler, K. F.; Stegmann, R.; Veldkamp, A.; Frenking, G. *Chem. Phys. Lett.* **1993**, *208*, 111.
- (35) Grimme, S. *J. Chem. Phys.* **2003**, *118*, 9095.
- (36) Tomasi, J.; Mennucci, B.; Cammi, R. *Chem. Rev.* **2005**, *105*, 2999.
- (37) Mammen, M.; Shakhnovich, E. I.; Deutch, J. M.; Whitesides, G. M. *J. Org. Chem.* **1998**, *63*, 3821.
- (38) Frisch, M. J.; et al. *Gaussian 09*, revision B.01; Gaussian, Inc.: Wallingford, CT, 2010.
- (39) Frey, G. D.; Lavallo, V.; Donnadieu, B.; Schoeller, W. W.; Bertrand, G. *Science* **2007**, *316*, 439.
- (40) (a) Sakaki, S.; Musashi, Y. *J. Chem. Soc., Dalton Trans.* **1994**, 3047. (b) Hutschka, F.; Dedieu, A.; Eichberger, M.; Fornika, R.; Leitner, W. *J. Am. Chem. Soc.* **1997**, *119*, 4432.
- (41) (a) Ohnishi, Y.; Matsunaga, T.; Nakao, Y.; Sato, H.; Sakaki, S. *J. Am. Chem. Soc.* **2005**, *127*, 4021. (b) Ohnishi, Y.; Nakao, Y.; Sato, H.; Sakaki, S. *Organometallics* **2006**, *25*, 3352.
- (42) The bond energies were defined as the energy difference between the fully optimized total system and their fragments with the frozen geometries.
- (43) Ferro, L.; Hitchcock, P. B.; Coles, M. P.; Cox, H.; Fulton, J. R. *Inorg. Chem.* **2011**, *50*, 1879.
- (44) Electron population was calculated with the frozen geometry taken from that of $\text{TS}_{2,1}\text{-SiMe}_3\text{H}$, where the Me groups are replaced with H or F. Only that moiety was reoptimized, to make consistent comparison with different silanes.
- (45) (a) Sakaki, S.; Aizawa, T.; Koga, N.; Morokuma, K.; Ohkubo, K. *Inorg. Chem.* **1989**, *28*, 103. (b) Sakaki, S.; Ohkubo, K. *Inorg. Chem.* **1989**, *28*, 2583.
- (46) Electron population was calculated with the fully optimized geometries of $\text{TS}_{2,1}\text{-SiF}_3\text{H}$ and $\text{TS}_{11,1}\text{-SiF}_3\text{H}$.
- (47) The $\text{C}=\text{N}$ π^* -antibonding MO energy of imine ($\text{RR}'\text{C}=\text{NH}$) becomes lower in the order of $(\text{CH}_3)_2\text{C}=\text{NH}$ (+4.46 eV) > $\text{CF}_3\text{CH}_2\text{C}=\text{NH}$ (+3.45 eV) > $(\text{CF}_3)_2\text{C}=\text{NH}$ (+2.21 eV).
- (48) Because the N atom of **12** has only one lone-pair orbital, the direction of the interaction with silane is limited, which leads to large steric repulsion. The direction of the interaction between the O atom and silane is more flexible in Ge(II) formate **11** and Ge(II) alkoxide **2** because the O atom has two lone-pair orbitals in **2** and **11**.